nature geoscience

SUPPLEMENTARY INFORMATION

https://doi.org/10.1038/s41561-019-0389-4

In the format provided by the authors and unedited.

Ice nucleation by aerosols from anthropogenic pollution

Bin Zhao[1,6*], Yuan Wang[2,3,6*], Yu Gu[1*], Kuo-Nan Liou[1], Jonathan H. Jiang[3], Jiwen Fan[4], Xiaohong Liu[5], Lei Huang[3] and Yuk L. Yung[2,3]

[1]Joint Institute for Regional Earth System Science and Engineering and Department of Atmospheric and Oceanic Sciences, University of California, Los Angeles, CA, USA. [2]Division of Geological and Planetary Sciences, California Institute of Technology, Pasadena, CA, USA. [3]Jet Propulsion Laboratory, California Institute of Technology, Pasadena, CA, USA. [4]Atmospheric Sciences and Global Change Division, Pacific Northwest National Laboratory, Richland, WA, USA. [5]Department of Atmospheric Science, University of Wyoming, Laramie, WY, USA. [6]These authors contributed equally: B. Zhao, Y. Wang. *e-mail: zhaob1206@ucla.edu; yuan.wang@caltech.edu; gu@atmos.ucla.edu

Supplementary Information

for "Ice nucleation by aerosols from anthropogenic pollution"

Bin Zhao[1,#,*], Yuan Wang[2,3,#,*], Yu Gu[1,*], Kuo-Nan Liou[1], Jonathan H. Jiang[3], Jiwen Fan[4], Xiaohong Liu[5], Lei Huang[3], and Yuk L. Yung[2,3]

[1]Joint Institute for Regional Earth System Science and Engineering and Department of Atmospheric and Oceanic Sciences, University of California, Los Angeles, California 90095, USA.

[2]Division of Geological and Planetary Sciences, California Institute of Technology, Pasadena, California 91109, USA.

[3]Jet propulsion Laboratory, California Institute of Technology, Pasadena, California 91109, USA.

[4]Atmospheric Sciences and Global Change Division, Pacific Northwest National Laboratory, Richland, Washington 99352, USA.

[5]Department of Atmospheric Science, University of Wyoming, Laramie, Wyoming 82071, USA.

[#]These authors contribute equally to this work.

*Correspondence to Bin Zhao (zhaob1206@ucla.edu), Yuan Wang (yuan.wang@caltech.edu), and Yu Gu (gu@atmos.ucla.edu)

1. Discussion of uncertainty in satellite retrievals

The satellite-derived ice particle effective radius (R_{ei}) and aerosol type have some intrinsic uncertainties. For R_{ei}, the MYD06 product provides an estimate of its uncertainty for each pixel, which takes into account a variety of error sources including 1) instrument calibration, 2) atmospheric corrections, 3) surface spectral reflectance, and 4) forward radiative transfer model, e.g., the size distribution assumption[1]. The pixel-level R_{ei} uncertainties for the samples used in this study are 6.5% ± 5.1% (standard deviation). In our analyses we use mean R_{ei} within certain AOD bins and the uncertainties should be smaller than those for individual pixels. Moreover, we focus on the changes of R_{ei} in response to aerosol loading rather than absolute R_{ei} values. For these reasons, we conclude that the uncertainty in R_{ei} retrieval is much smaller than the magnitude of R_{ei} changes with aerosol loading (see Fig. 1 and Fig. S2).

The aerosol types are primarily classified based on CALIOP, and further refined using retrievals of AIRS in this study. In the retrieval algorithm of CALIOP, depolarization ratio is one of the most important parameters used to distinguish dust (depolarization ratio > 0.2), polluted dust (0.075-0.2), and polluted continental aerosols (< 0.075)[2]. Based on measurements in more than 15 field campaigns, Burton et al.[3] reported that the depolarization ratio of pure dust ranges between 0.30 and 0.35 (5^{th} and 95^{th} percentiles), while that of urban aerosols (comparable to polluted continental aerosols in this study) ranges between 0.02 and 0.10. Many other field measurements also support the preceding ranges of depolarization ratio for the two aerosol types[3-10]. It is therefore safe to state that the algorithm can separate dust and polluted continental aerosols well.

A couple of studies have evaluated the aerosol classification in the Version 3 (old version) CALIOP product[11-13]. Tesche et al.[11] showed that the Cape Verde region aerosol type was reliably classified. Wu et al.[13] showed that the CALIOP algorithms for cloud-aerosol discrimination and

aerosol type classification generally work well over the New York metropolitan area, with a few exceptions where very dense smoke layers are misclassified as clouds or polluted dusts. Noted that these validation studies were based on the Version 3 CALIOP product. Our study uses the new CALIOP Version 4 aerosol product (released in November 2016) which includes substantial improvement in the aerosol subtyping and lidar ratio selection algorithms[2]. The new Version 4 product has addressed most aerosol typing concerns raised in the validation and application of Version 3 products, including the issue of dense smoke layers mentioned above[2]. The discussion above indicates that CALIOP classifies various aerosol types reasonably well.

It is noted that, in this study, soil dust is not classified as polluted continental aerosols, but classified as dust (when not contaminated by polluted continental aerosols) or polluted dust (when mixed with polluted aerosols). Similar to mineral dust, pure soil dust possesses irregular shape and hence relatively large depolarization ratio[14-16]. Since soil dust is usually mixed with more spherical aerosols from anthropogenic pollution, the depolarization ratio of soil dust detected in the atmosphere ranges between ~0.1 and 0.25[14-16], smaller than those of pure mineral dust (0.3-0.35[3-5]) but larger than those of polluted continental aerosols (< 0.075[3,6,7]).

2. Statistical method and result interpretation in correlation analyses

We have calculated the Pearson's partial correlation between AOD and R_{ei}, in order to exclude the impact of meteorological covariation. The partial correlation is a measure of the dependence between two variables where the influence from possible controlling variables (meteorological parameters in this case) is removed[17-20]. Let X denote a vector of meteorological parameters, the effects of which we would like to eliminate. The partial correlation between AOD and R_{ei}, eliminating the effects of X, is:

$$R_{AOD-Rei.X} = \frac{\sigma_{AOD-Rei.X}}{\sigma_{AOD.X}\sigma_{Rei.X}} \quad (1)$$

where $\sigma_{AOD-Rei.X}$ is the conditional covariance between AOD and R_{ei}, eliminating effects of X; $\sigma_{AOD.X}$ is the square root of the conditional variance of AOD, eliminating effects of X; $\sigma_{Rei.X}$ is the square root of the conditional variance of R_{ei}, eliminating effects of X.

If X is a single meteorological parameter, Eq 1 is reduced to Eq 2:

$$R_{AOD-Rei.X} = \frac{R_{AOD-Rei} - R_{AOD-X} \cdot R_{Rei-X}}{\sqrt{1-R_{AOD-X}^2}\sqrt{1-R_{Rei-X}^2}} \quad (2)$$

where $R_{AOD-Rei}$ is the Pearson's total correlation between AOD and R_{ei}; R_{AOD-X} is the Pearson's total correlation between AOD and X; $R_{\mathrm{Rei}-X}$ is the Pearson's total correlation between R_{ei} and X.

Considering that the relationships between AOD and R_{ei} may not be linear, we have also calculated the Spearman's correlation, which is a nonparametric measure of statistical dependence between the rankings of two variables. The Spearman's correlation between two variables is equal to the Pearson's correlation between the rank values of those two variables. Similar to the Pearson's partial correlation, we also calculate the Spearman's partial correlation. The Spearman's partial correlation is defined and calculated in the same way as the Pearson's partial correlation (Eqs. 1 and 2) except that the original variables should be replaced by their rank values in the calculation. More details of the definition and calculation for partial correlation are described in other references[18-22]. In this study, the Pearson's and Spearman's correlation and partial correlation are all calculated using the "corr" and "partialcorr" functions in MATLAB.

Thirteen meteorological parameters (see Methods) are chosen in the correlation analysis, because they could influence the formation and evolution of convective clouds and convection-generated anvil cirrus. Relative humidity is an indicator of water vapor amount and directly controls the formation and growth of both liquid cloud droplets and ice particles. CAPE is a measure of maximal energy available for convection to consume, while CIN represents the maximal energy that prevents the development of convection. Although mid-latitude strong

convection is not necessarily characterized by high CAPE/low CIN, the large-scale instability indicated by high CAPE and/or low CIN favors the development of convective clouds. The vertical velocity informs atmospheric dynamic condition. High vertical velocity results in a faster development of supersaturation and hence accelerated production of liquid droplets or ice particles. Horizontal wind speed and direction denote the origin of air mass at the location of clouds. For example, when easterly wind prevails, the air mass in East Asia more likely comes from the moist Pacific Ocean, while it is more likely to be from the dry inland continent when wind direction reverses. The distinct physical properties of air masses such as moisture content subsequently affect the ice particle formation and growth. Finally, an optimal strength of vertical wind shear can help organize convective systems and extend their lifetimes[23], which further impacts the lifecycle of ice particles.

The results of the Pearson's total and partial correlations have been described in the main text. The results of Spearman's total and partial correlations are summarized in Fig. S5. We find that the Spearman's total and partial correlations are very similar to the Pearson's total and partial correlations, except that the magnitude of the former (Spearman's) is slightly larger than the latter.

The magnitude of the correlations is not large, since R_{ei} is affected by many factors other than aerosols. However, all Pearson's and Spearman's total and partial correlations are statistically significant at the 0.01 level based on the Student's t-test. In addition, over 90% of the Pearson's (total and partial) correlations and 99% of the Spearman's correlations are significant at the 0.001 level. Actually, small correlations between aerosol loading and ice/mixed-phase cloud properties have also been documented in previous studies that used satellite products. For example, the correlations between AOD and specific cloud properties are: 0.03-0.17 for cloud fraction[20], 0.03-0.25 for cloud thickness[20], 0.08-0.20 for cloud optical thickness[20], and 0.02-0.18 for ice mass-

111 weighted altitude centroid[24]. Therefore, the small correlation coefficients do not affect the
112 robustness of aerosol impacts on cloud properties investigated in this study.

113 Figures 2 and S4 show that the magnitude of R_{ei}-AOD correlations for polluted continental
114 aerosols is larger than that for dust, for subsets with > 67% percentile CTH or < 33% percentile
115 CTH. In contrast, the correlations for dust are often larger than polluted continental aerosols for
116 subsets with > 67% percentile CAPE or < 33% percentile CAPE. The reason for the difference is
117 complicated. Our additional analyses suggest that it is possibly caused by the different vertical
118 distributions of dust and polluted continental aerosols. Compared with polluted continental
119 aerosols, a larger fraction of dust is usually located at higher altitude, as shown in previous
120 studies[25,26].

121 Specifically, while CTH and CAPE are both indicators of convective strength, the samples
122 with > 67% percentile CTH and > 67% percentile CAPE are not exactly the same. The samples
123 that belong to the > 67% CTH group but not belong to the > 67% CAPE group are characterized
124 by a high altitude (> 67% percentile CTH) but relatively higher thermodynamic stability (< 67%
125 percentile CAPE). In such conditions, aerosols in the upper troposphere may have a stronger effect
126 on clouds than those near the ground surface. Considering that a smaller fraction of polluted
127 continental aerosols resides in the upper troposphere than dust, the available amount of polluted
128 continental aerosols that interact with clouds is smaller. For this reason, R_{ei} is more sensitive to a
129 change in AOD of polluted continental aerosols, leading to a larger negative correlation for
130 polluted continental aerosols.

131 In contrast, the samples that belong to the > 67% CAPE group but not belong to the > 67%
132 CTH group are characterized by a strong instability (> 67% percentile CAPE) but relatively low
133 height (< 67% percentile CTH). In such conditions, clouds are probably more affected by aerosols

at lower altitude, where polluted continental aerosols tend to be more abundant than dust. Therefore, R_{ei} is more sensitive to a change in dust aerosols (i.e., a larger negative correlation for dust).

Similarly, we compare the groups with < 33% percentile CTH and < 33% percentile CAPE. The samples that belong to the < 33% CTH group but not belong to the < 33% CAPE group reside in a low altitude (< 33% percentile CTH) but with relatively strong instability (> 33% percentile CAPE). In this case, clouds are strongly affected by aerosols at lower heights where polluted continental aerosols are more abundant than dust. As a result, when homogeneous freezing dominates (i.e., the small AOD range), R_{ei} is smaller for clouds mixed with polluted continental aerosols than those mixed with dust. When heterogeneous nucleation overtakes homogeneous with an increase in AOD, the increase in R_{ei} is thus larger for clouds mixed with polluted continental aerosols. This produces a larger positive correlation for polluted continental aerosols.

3. Justification of using R_{ei} near cloud top

MODIS-retrieved R_{ei} is dominated by ice particles near cloud top. The use of R_{ei} near cloud top is justified by the following reasons.

First, in our analysis, we are not tracking the formation and lifecycle of ice particles, but focusing on the net effect of the competition between different ice nucleation pathways. This net effect can only be reflected by the R_{ei} in cloud layers above the height of −37 °C isotherm. The temperature threshold applied here is to include the influence of homogeneous freezing, which is the key to studying the competition between different ice nucleation pathways.

Second, ice particles near cloud top should be able to represent ice particles in the cloud layers colder than −37 °C, as those layers are presumably much thinner than the total thickness of convective clouds. To test such an assumption, we have compared two different methods to

calculate R_{ei} in our model simulations. In the first method, we use the ice particles only from the top layer of the cloud (Fig. S8). In the second method, we use ice particles at all layers above the height of −37 °C isotherm (Fig. 3). The comparison shows that the R_{ei}-aerosol relationships are roughly unchanged by different choices of cloud layers above the −37 °C isotherm.

4. Possible constituents of anthropogenic aerosols serving as INPs

An unresolved question in this study is what constituents contribute a major fraction of the INPs from anthropogenic pollution. Organic aerosol is a potential candidate[27]. A unique feature of organic aerosol is that it is mostly amorphous and can exist in liquid, semisolid, and solid (glassy) states in response to changes in temperature and relative humidity[27,28]. At glassy state, it could serve as INPs for deposition nucleation. During the transition from glassy to liquid states, a residual solid core is coated by an aqueous shell, and immersion freezing may proceed[27,29]. Such a transitional state could commonly exist in developing clouds as the time scale for solid-to-liquid transition are mostly longer than typical cloud activation time periods[27,28]. Aside from organic aerosols, lead-bearing aerosols have been shown to be among the most efficient ice-forming substances commonly found in the atmosphere, as evidenced by the dramatically enhanced concentrations in ice residuals compared to near-cloud aerosols, as well as by laboratory experiments[30-32]. Lead predominantly originates from anthropogenic sources including fossil fuel combustion and industrial processes[33]. For black carbon (or soot) particles, some studies showed their ability to catalyze ice nucleation at temperatures much warmer than −37°C, although conflicting results also exist[34-37]. A possible reason for the disagreement among various studies is that the ice nucleation efficiency of carbonaceous aerosol depends significantly on a number of factors, including hygroscopicity[38,39], organic carbon content[40], chemical aging[41], and mesopore structure[36]. Further research is needed to reconcile the contradicting results and to elucidate the

underlying control factors. Other anthropogenic aerosol constituents serving as INPs have been discussed, such as solid ammonium sulfate[42] and metallic compounds (other than lead)[43].

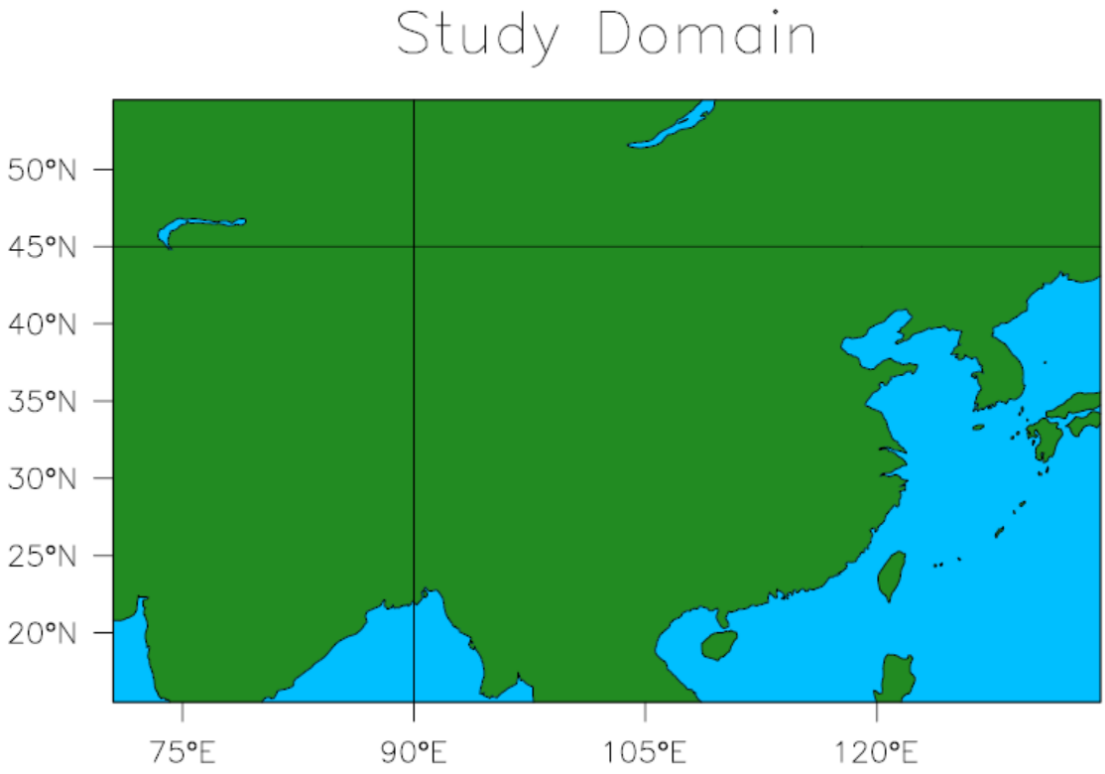

Figure S1. Illustration of the spatial domain of this study (15-55 N, 70-135 E).

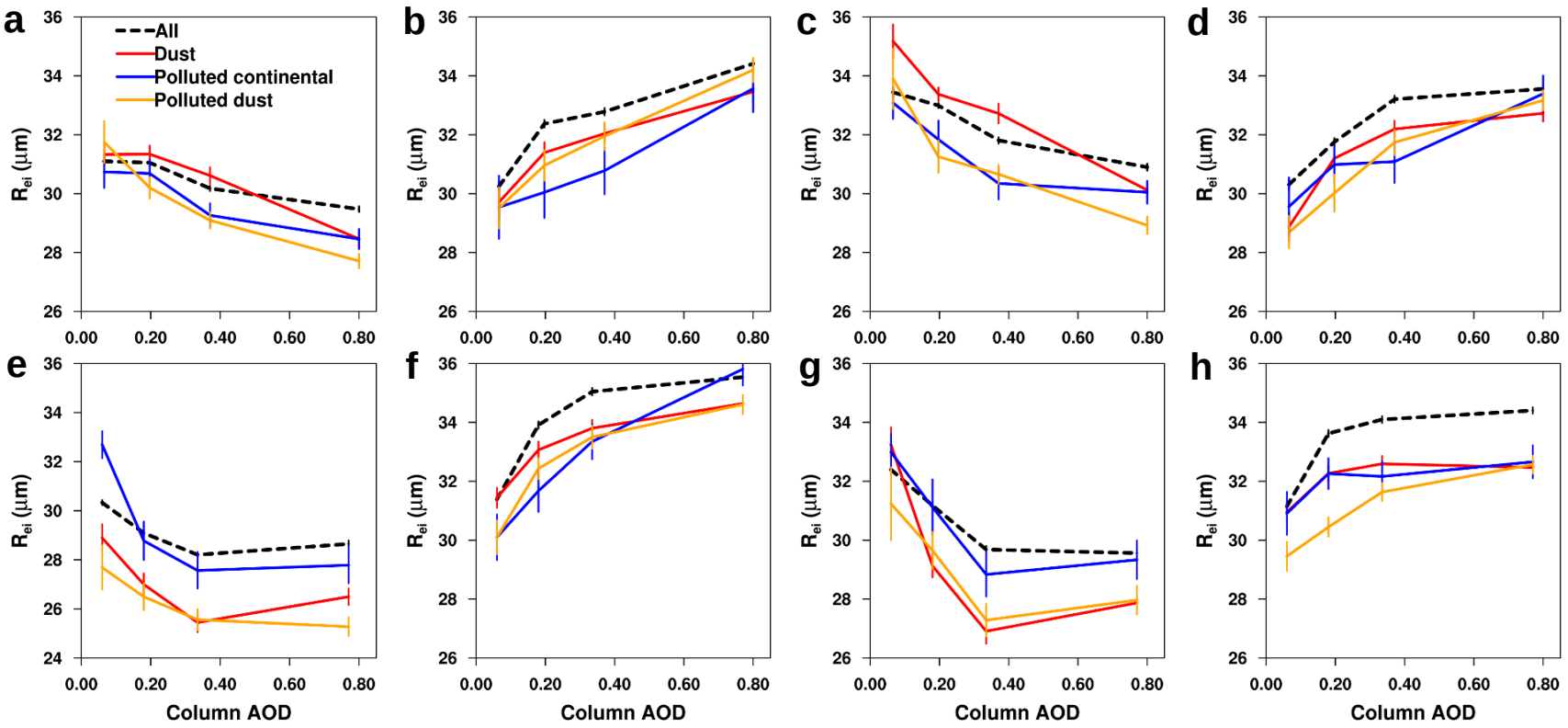

Figure S2. Relationships between column AOD and R_{ei} of cold-top convective clouds (a-d) and anvil cirrus clouds (e-h) with different ranges of cloud top height (CTH) or surface-based CAPE: (a, e) > 67% percentile of CTH, (b, f) < 33% percentile of CTH, (c, g) > 67% percentile of CAPE, and (d, h) < 33% percentile of CAPE. The division of AOD bins and the definition of error bars are the same as in Fig. 1.

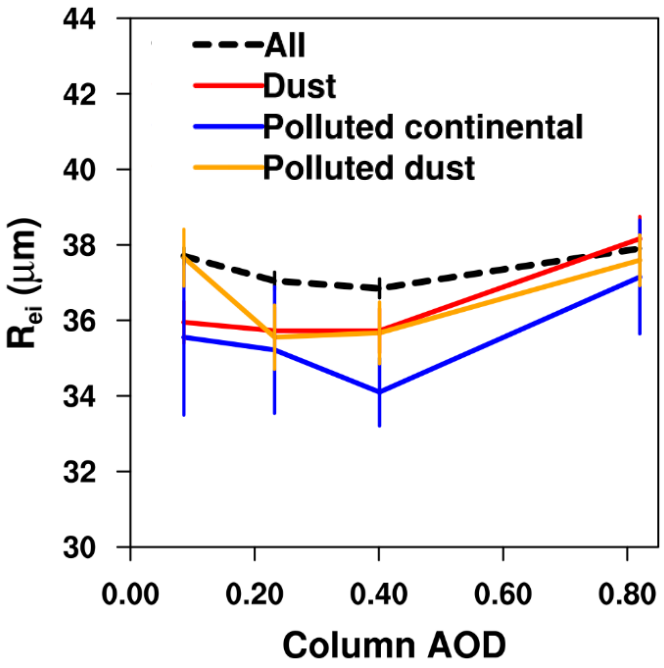

Figure S3. Relationships between AOD and R_{ei} of warm-top convective clouds (cloud top temperature > −30 ºC). The division of AOD bins and the definition of error bars are the same as in Fig. 1.

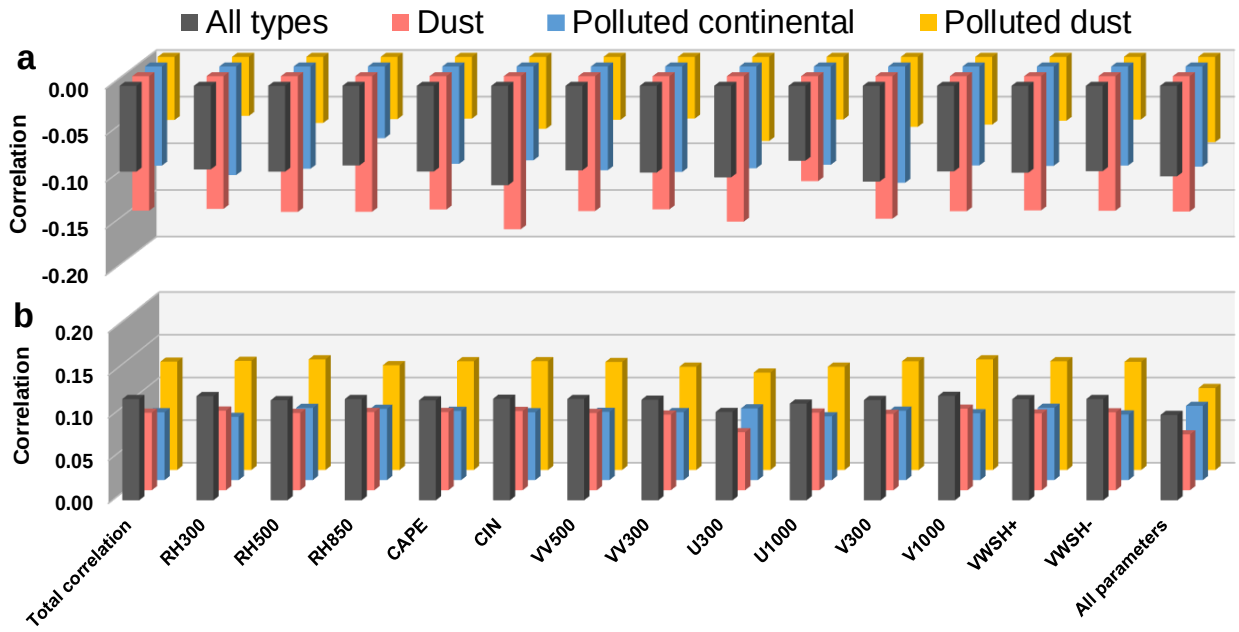

Figure S4. The same as Fig. 2 but for (a) > 67% percentile of CAPE, and (b) < 33% percentile of CAPE.

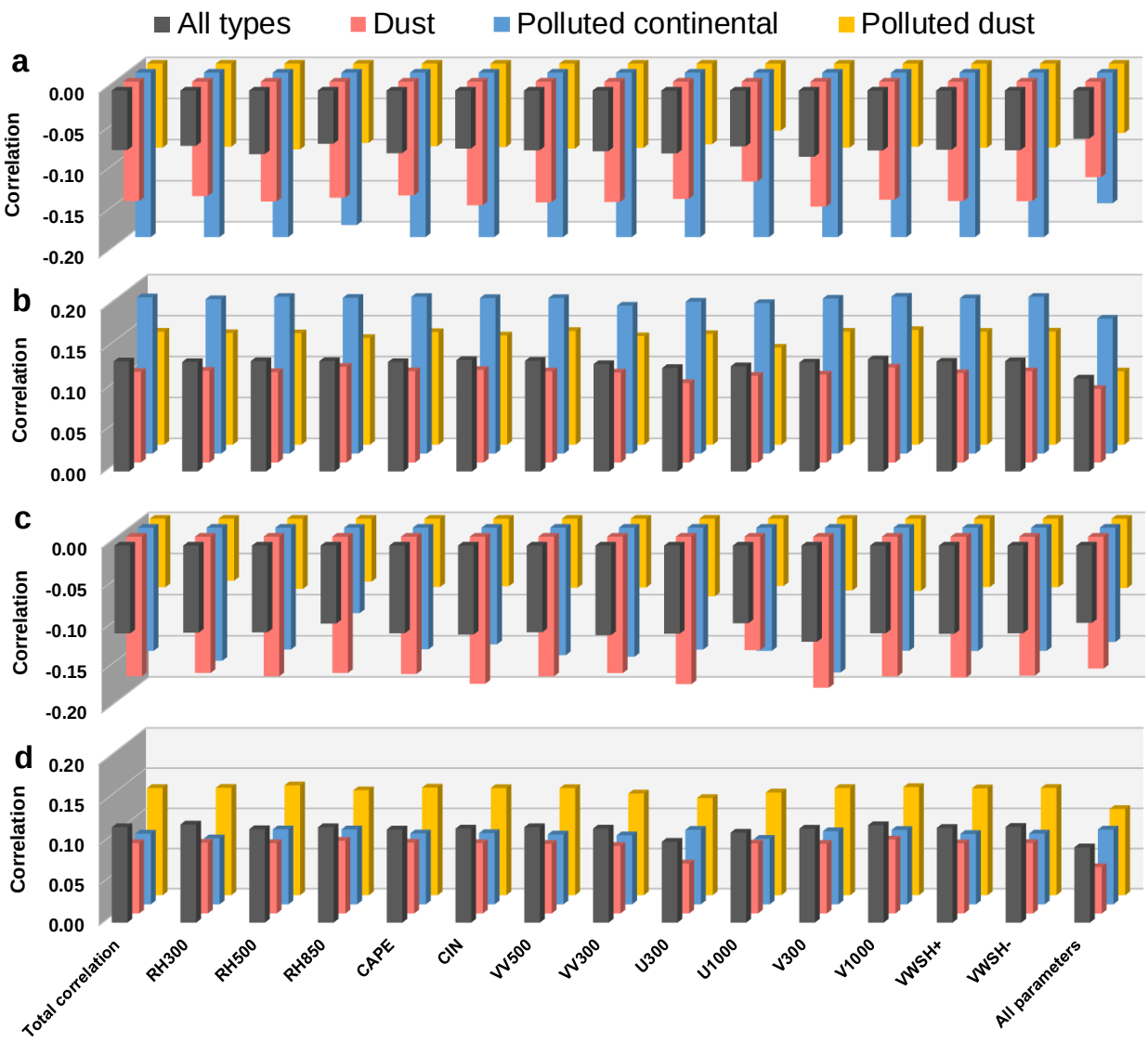

Figure S5. Spearman's (total) correlations between AOD and R_{ei} (the leftmost column in each panel), and Spearman's partial correlations with the effects of listed meteorological parameters eliminated all simultaneously (the rightmost column in each panel) and individually (the in-between columns in each panel): (a) > 67% percentile of CTH, (b) < 33% percentile of CTH, (c) > 67% percentile of CAPE, and (d) < 33% percentile of CAPE. All correlations presented in this figure are statistically significant at the 0.01 level. AOD range is [0, 0.8].

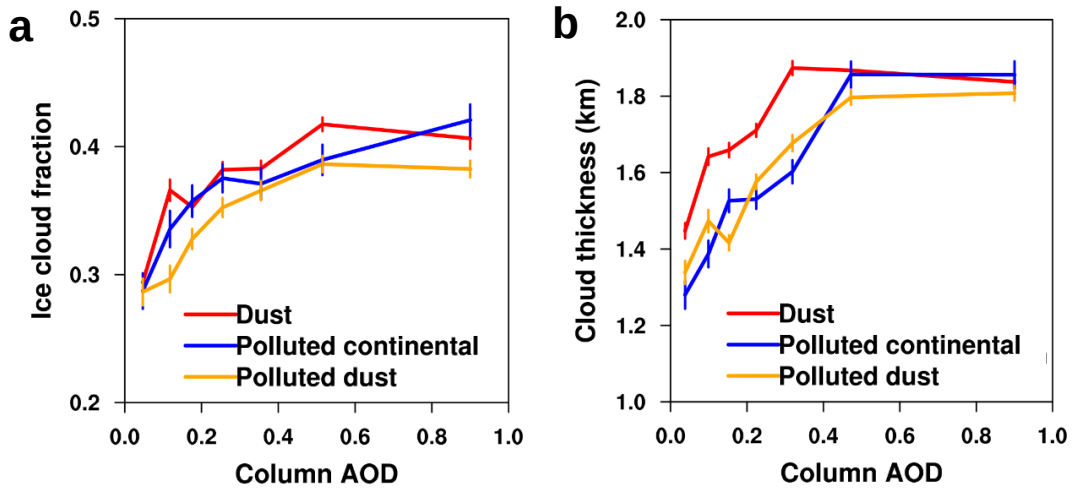

205

206 **Figure S6**. Changes in ice cloud fraction (a) and cloud thickness (b) of anvil cirrus clouds with
207 AOD for different aerosol types. The division of AOD bins and the definition of error bars are the
208 same as in Fig. 1.

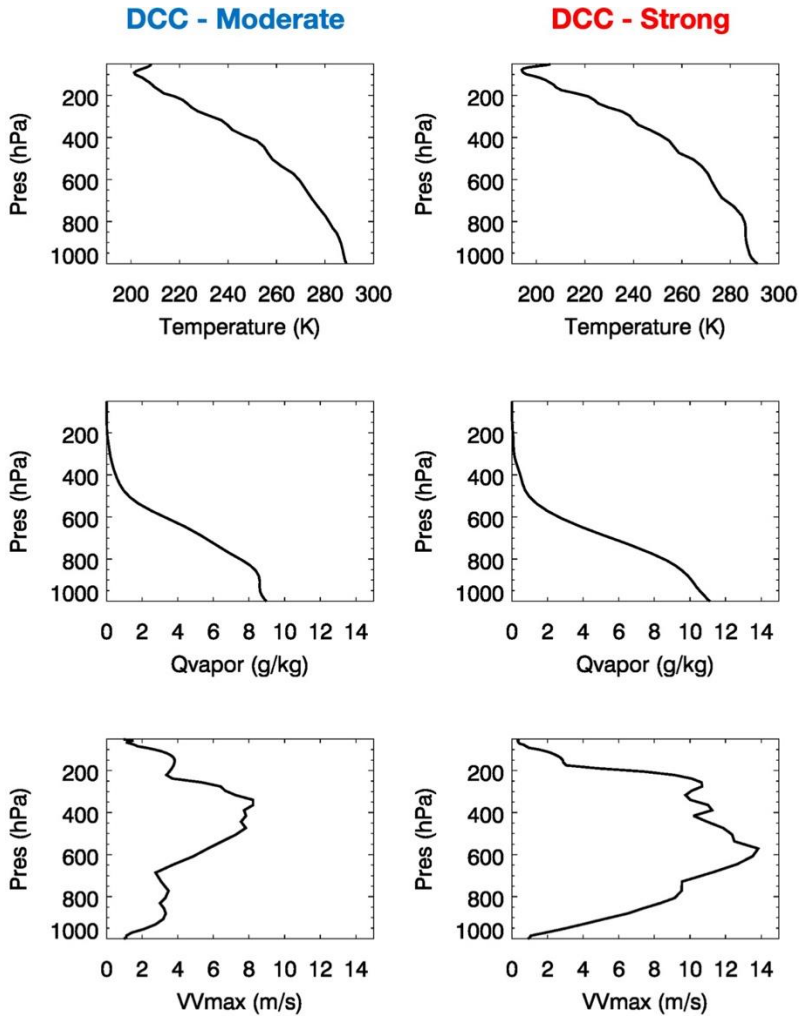

209

210 **Figure S7**. WRF simulated temperature, specific humidity (Qvapor), and maximal updraft velocity
211 (VVmax) in two cases. The results are averaged over the whole domain and over a 12-hour window
212 centering at the peak of the convections.

213

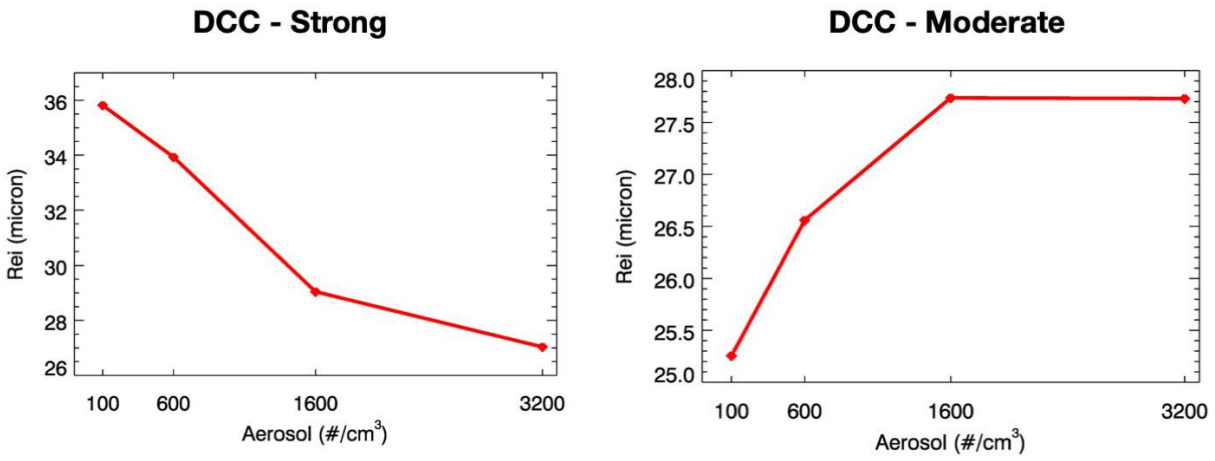

Figure S8. The same with Fig. 3a,c, but using the top layer of clouds to calculate R_{ei}.

Table S1. Datasets used in this study.

Satellite/ Sensor	Product	Variable	Horizontal resolution
Aqua/MODIS	MYD04 (Level 2, Collection 6)	Column AOD	10 km × 10 km
	MYD06 (Level 2, Collection 6)	Cloud effective radius, cloud phase (determined by the "cloud optical property" algorithm), primary cloud retrieval outcome, cloud effective radius uncertainty	1 km × 1 km
CALIPSO/ CALIOP	05kmMLay (Level 2, Version 4.10)	Aerosol/cloud layer number, layer top/base temperature, layer top/base height, feature classification flags (containing "aerosol type" and "cloud type" flags), CAD score, extinction QC	5 km along-track
	05kmAPro (Level 2, Version 4.10)	Vertically resolved pressure, relative humidity, and temperature	5 km along-track
Aqua/AIRS	AIRIBRAD	Dust_score	13.5 km × 13.5 km
--	NCEP Final Analysis (ds083.2)	Vertically resolved pressure vertical velocity and wind speed; CAPE, CIN, wind shear	1 º × 1 º

References

1 Platnick, S., King, M. D. & Meyer, K. G. *MODIS cloud optical properties: user guide for the collection 6 level-2 MOD06/MYD06 product and associated level-3 datasets*, <https://modis-images.gsfc.nasa.gov/_docs/C6MOD06OPUserGuide.pdf> (2015).

2 Kim, M. H. *et al.* The CALIPSO version 4 automated aerosol classification and lidar ratio selection algorithm. *Atmos. Meas. Tech.* **11**, 6107-6135 (2018).

3 Burton, S. P. *et al.* Aerosol classification using airborne High Spectral Resolution Lidar measurements - methodology and examples. *Atmos. Meas. Tech.* **5**, 73-98 (2012).

4 Liu, Z. Y. *et al.* CALIPSO lidar observations of the optical properties of Saharan dust: A case study of long-range transport. *J. Geophys. Res-Atmos.* **113**, D07207 (2008).

5 Freudenthaler, V. *et al.* Depolarization ratio profiling at several wavelengths in pure Saharan dust during SAMUM 2006. *Tellus. B.* **61**, 165-179 (2009).

6 Gobbi, G. P., Barnaba, F., Blumthaler, M., Labow, G. & Herman, J. R. Observed effects of particles nonsphericity on the retrieval of marine and desert dust aerosol optical depth by lidar. *Atmos. Res.* **61**, 1-14 (2002).

7 Sakai, T. *et al.* Raman lidar and aircraft measurements of tropospheric aerosol particles during the Asian dust event over central Japan: Case study on 23 April 1996. *J. Geophys. Res-Atmos.* **108**, 4349 (2003).

8 Murayama, T. *et al.* An intercomparison of lidar-derived aerosol optical properties with airborne measurements near Tokyo during ACE-Asia. *J. Geophys. Res-Atmos.* **108**, 8651 (2003).
9 Shimizu, A. *et al.* Continuous observations of Asian dust and other aerosols by polarization lidars in China and Japan during ACE-Asia. *J. Geophys. Res-Atmos.* **109**, D19s17 (2004).
10 Gobbi, G. P., Barnaba, F., Giorgi, R. & Santacasa, A. Altitude-resolved properties of a Saharan dust event over the Mediterranean. *Atmos. Environ.* **34**, 5119-5127 (2000).
11 Tesche, M. *et al.* Ground-based validation of CALIPSO observations of dust and smoke in the Cape Verde region. *J. Geophys. Res-Atmos.* **118**, 2889-2902 (2013).
12 Mielonen, T. *et al.* Comparison of CALIOP level 2 aerosol subtypes to aerosol types derived from AERONET inversion data. *Geophys. Res. Lett.* **36**, L18804 (2009).
13 Wu, Y. H., Cordero, L., Gross, B., Moshary, F. & Ahmed, S. Assessment of CALIPSO attenuated backscatter and aerosol retrievals with a combined ground-based multi-wavelength lidar and sunphotometer measurement. *Atmos. Environ.* **84**, 44-53 (2014).
14 Huang, J. P., Liu, J. J., Chen, B. & Nasiri, S. L. Detection of anthropogenic dust using CALIPSO lidar measurements. *Atmos. Chem. Phys.* **15**, 11653-11665 (2015).
15 Nemuc, A., Vasilescu, J., Talianu, C., Belegante, L. & Nicolae, D. Assessment of aerosol's mass concentrations from measured linear particle depolarization ratio (vertically resolved) and simulations. *Atmos. Meas. Tech.* **6**, 3243-3255 (2013).
16 Nisantzi, A., Mamouri, R. E., Ansmann, A. & Hadjimitsis, D. Injection of mineral dust into the free troposphere during fire events observed with polarization lidar at Limassol, Cyprus. *Atmos. Chem. Phys.* **14**, 12155-12165 (2014).
17 Engstrom, A. & Ekman, A. M. L. Impact of meteorological factors on the correlation between aerosol optical depth and cloud fraction. *Geophys. Res. Lett.* **37**, L18814 (2010).
18 Hardle, W. K. & Simar, L. *Applied Multivariate Statistical Analysis, fourth edition*. 773 (Springer, 2015).
19 Johnson, R. A. & Wichern, D. W. *Applied Multivariate Statistical Analysis, sixth edition*. 773 (Pearson Education Inc., 2007).
20 Zhao, B. *et al.* Type-Dependent Responses of Ice Cloud Properties to Aerosols From Satellite Retrievals. *Geophys. Res. Lett.* **45**, 3297-3306 (2018).
21 PSU. *STAT 505 - Applied Multivariate Statistical Analysis, available at https://onlinecourses.science.psu.edu/stat505/*, 2017).
22 Sprent, P. & Smeeton, N. C. *Applied Nonparametric Statistical Methods, Third Edition*. 463 (Chapman & Hall/CRC, 2001).
23 Amber, U., Wang, S. G. & Sobel, A. Response of Atmospheric Convection to Vertical Wind Shear: Cloud-System-Resolving Simulations with Parameterized Large-Scale Circulation. Part I: Specified Radiative Cooling. *J. Atmos. Sci.* **71**, 2976-2993 (2014).
24 Jiang, J. H. *et al.* Contrasting effects on deep convective clouds by different types of aerosols. *Nat. Commun.* **9**, 3874 (2018).
25 Zhao, B. *et al.* Intra-annual variations of regional aerosol optical depth, vertical distribution, and particle types from multiple satellite and ground-based observational datasets. *Atmos. Chem. Phys.* **18**, 11247-11260 (2018).
26 Huang, L., Jiang, J. H., Tackett, J. L., Su, H. & Fu, R. Seasonal and diurnal variations of aerosol extinction profile and type distribution from CALIPSO 5-year observations. *J. Geophys. Res-Atmos.* **118**, 4572-4596 (2013).

27 Knopf, D. A., Alpert, P. A. & Wang, B. B. The Role of Organic Aerosol in Atmospheric Ice Nucleation: A Review. *ACS. Earth. Space. Chem.* **2**, 168-202 (2018).
28 Shiraiwa, M. *et al.* Global distribution of particle phase state in atmospheric secondary organic aerosols. *Nat. Commun.* **8**, 15002 (2017).
29 China, S. *et al.* Ice cloud formation potential by free tropospheric particles from long-range transport over the Northern Atlantic Ocean. *J. Geophys. Res-Atmos.* **122**, 3065-3079 (2017).
30 Cziczo, D. J. *et al.* Inadvertent climate modification due to anthropogenic lead. *Nat. Geosci.* **2**, 333-336 (2009).
31 Ebert, M. *et al.* Chemical composition and mixing-state of ice residuals sampled within mixed phase clouds. *Atmos. Chem. Phys.* **11**, 2805-2816 (2011).
32 Kamphus, M. *et al.* Chemical composition of ambient aerosol, ice residues and cloud droplet residues in mixed-phase clouds: single particle analysis during the Cloud and Aerosol Characterization Experiment (CLACE 6). *Atmos. Chem. Phys.* **10**, 8077-8095 (2010).
33 Tian, H. Z. *et al.* Quantitative assessment of atmospheric emissions of toxic heavy metals from anthropogenic sources in China: historical trend, spatial distribution, uncertainties, and control policies. *Atmos. Chem. Phys.* **15**, 10127-10147 (2015).
34 Bond, T. C. *et al.* Bounding the role of black carbon in the climate system: A scientific assessment. *J. Geophys. Res-Atmos.* **118**, 5380-5552 (2013).
35 Hoose, C. & Moehler, O. Heterogeneous ice nucleation on atmospheric aerosols: a review of results from laboratory experiments. *Atmos. Chem. Phys.* **12**, 9817-9854 (2012).
36 Mahrt, F. *et al.* Ice nucleation abilities of soot particles determined with the Horizontal Ice Nucleation Chamber. *Atmos. Chem. Phys.* **18**, 13363-13392 (2018).
37 Charnawskas, J. C. *et al.* Condensed-phase biogenic-anthropogenic interactions with implications for cold cloud formation. *Faraday. Discuss.* **200**, 165-194 (2017).
38 Gorbunov, B., Baklanov, A., Kakutkina, N., Windsor, H. L. & Toumi, R. Ice nucleation on soot particles. *J. Aerosol. Sci.* **32**, 199-215 (2001).
39 Koehler, K. A. *et al.* Cloud condensation nuclei and ice nucleation activity of hydrophobic and hydrophilic soot particles. *Phys. Chem. Chem. Phys.* **11**, 7906-7920 (2009).
40 Crawford, I. *et al.* Studies of propane flame soot acting as heterogeneous ice nuclei in conjunction with single particle soot photometer measurements. *Atmos. Chem. Phys.* **11**, 9549-9561 (2011).
41 Brooks, S. D., Suter, K. & Olivarez, L. Effects of Chemical Aging on the Ice Nucleation Activity of Soot and Polycyclic Aromatic Hydrocarbon Aerosols. *J. Phys. Chem. A.* **118**, 10036-10047 (2014).
42 Hung, H. M., Malinowski, A. & Martin, S. T. Ice nucleation kinetics of aerosols containing aqueous and solid ammonium sulfate particles. *J. Phys. Chem. A.* **106**, 293-306 (2002).
43 Kanji, Z. A. *et al.* Overview of Ice Nucleating Particles. in *Ice Formation and Evolution in Clouds and Precipitation: Measurement and Modeling Challenges* Vol. 58 1.1-1.33 (American Meteorological Society, 2017).